Supporting Information

Co-sintering Reaction Analysis of $LiCoO_2$ Cathodes and NASICON-Type LATP Solid Electrolytes Studied by Experimental and Computational Methods

Fumihiko Ichihara[†], Shogo Miyoshi[†], Machiko Ode[‡] and Takuya Masuda[†§]*

† Research Center for Energy and Environmental Materials, National Institute for Materials Science (NIMS), Tsukuba, Ibaraki 305-0044, Japan.

‡ Research Center for Structural Materials, National Institute for Materials Science (NIMS), Tsukuba, Ibaraki 305-0047, Japan.

§ Graduate School of Chemical Sciences and Engineering, Hokkaido University, Sapporo, Hokkaido 060-0810, Japan.

1. XRD data analysis

Table S1. Powder diffraction files for Rietveld analysis.

Chemical Species	Chemical Formula	Crystal Structure	Powder Diffraction File card number	ICSD
Lithium cobalt oxide	$LiCoO_2$	R-3m	01-070-2685	51182
Lithium dititanium tris(phosphate(V))	$LiTi_2(PO_4)_3$	R-3c	01-072-6140	95979
Cobalt oxide	Co_3O_4	Fd-3m	01-076-1802	36256
Lithiophosphate	Li_3PO_4	Pmnb	01-087-0039	50058
Cobalt titanium oxide	$CoTiO_3$	R-3h	01-077-1373	48107
Titanium oxide, rutile	TiO_2	$P4_2/mnm$	01-070-7347	093097
Lithium cobalt phosphate(V), olivine	$LiCoPO_4$	Pnma	01-089-6192	87422
Dicobalt titanium Oxide	Co_2TiO_4	Fd-3m	01-080-1671	69506
Dilithium titanate	Li_2TiO_3	C2/c	01-080-7162	261238

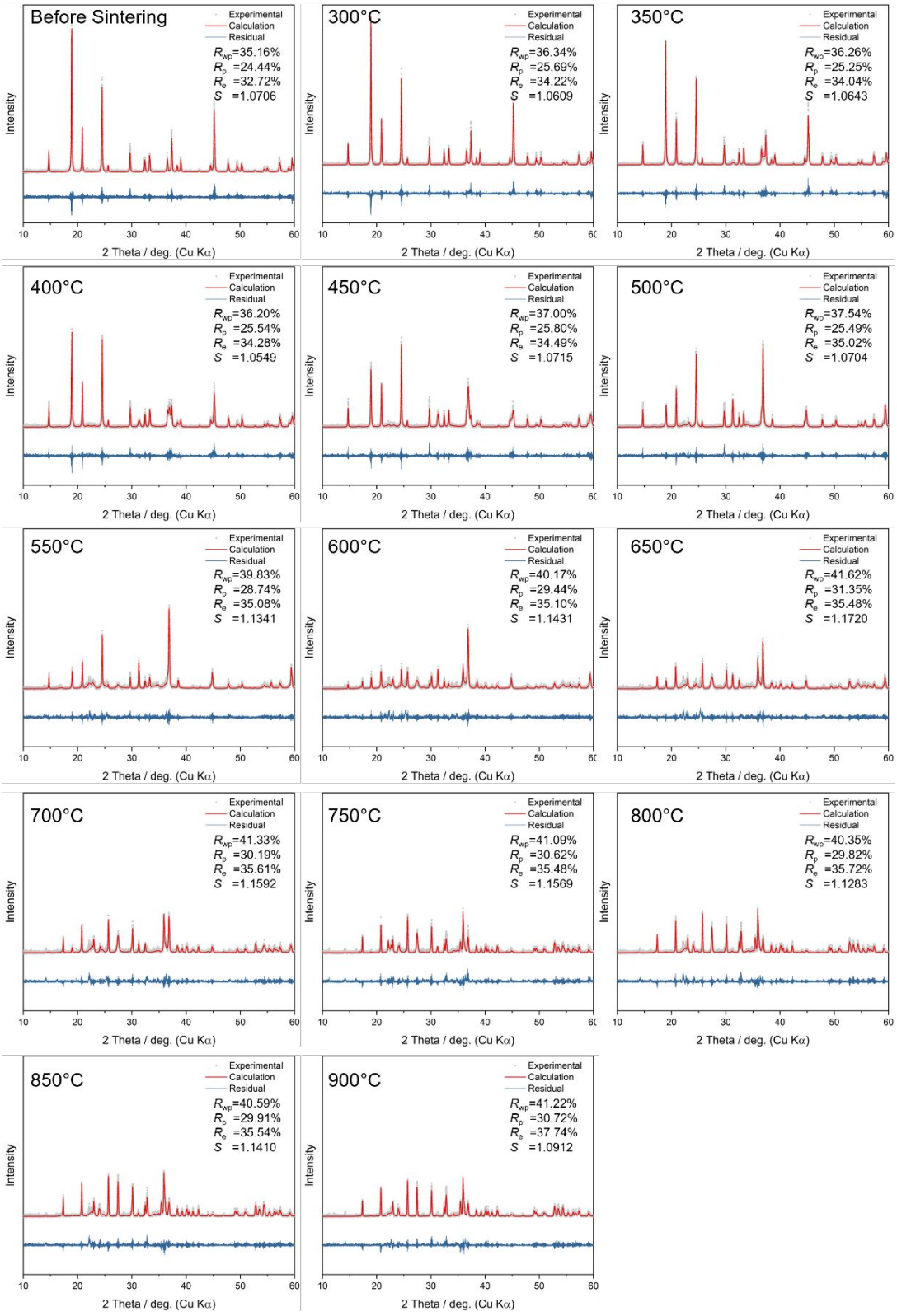

Figure S1. Results of Rietveld analysis of XRD patterns derived from LCLA37.

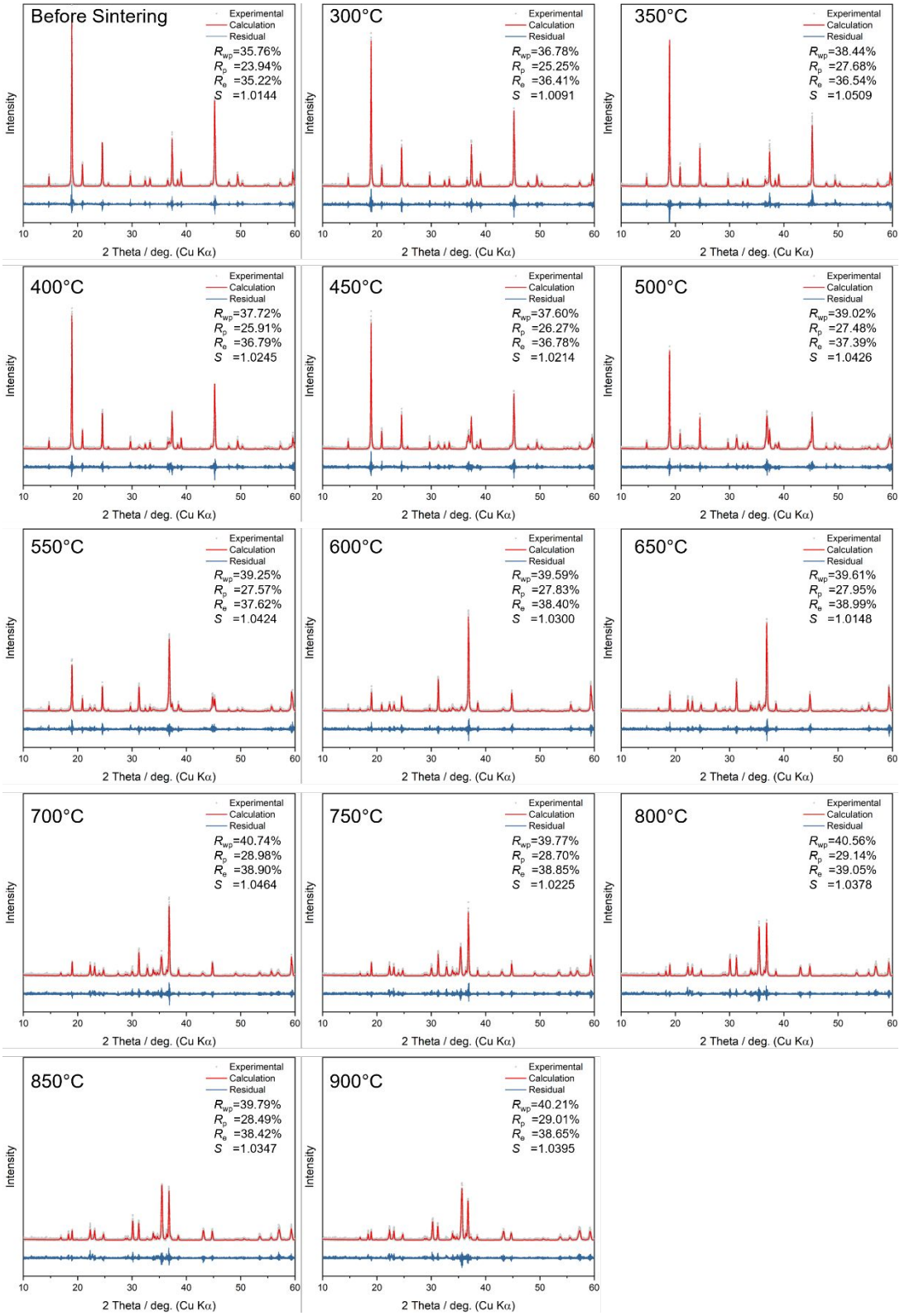

Figure S2. Results of Rietveld analysis of XRD patterns derived from LCLA55.

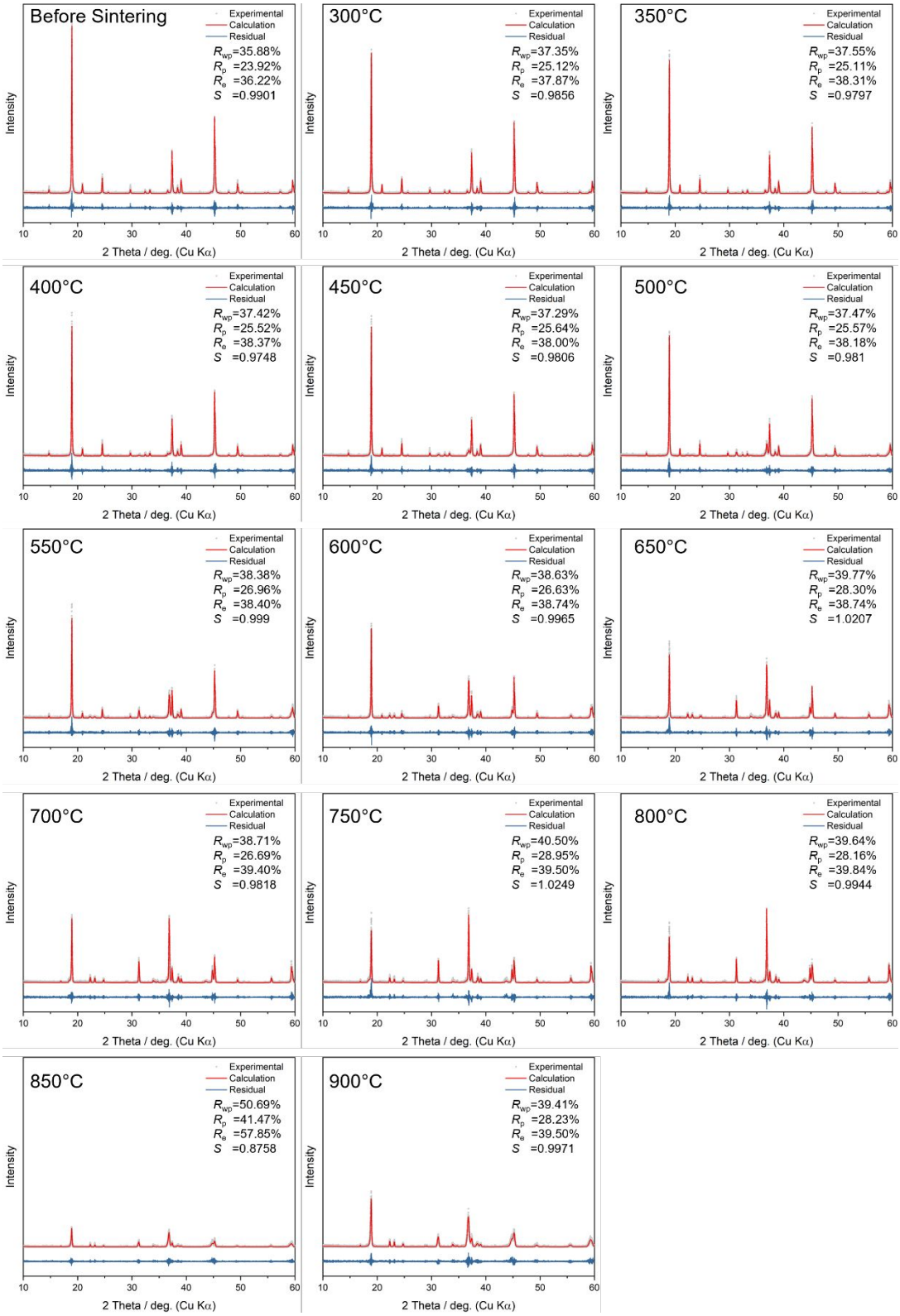

Figure S3. Results of Rietveld analysis of XRD patterns derived from LCLA73.

2. XANES data analysis

Table S2. Principal component analysis results for Co K-edge XANES spectra of LCLA37.

Components	Eigenvalues	Variance	Cumulative variance
1	13.22671	0.944765	0.944765
2	0.745323	0.053237	0.998003
3	0.026473	0.001891	0.999893
4	0.000819	0.000059	0.999952
5	0.000374	0.000027	0.999979
6	0.000167	0.000012	0.999991
7	0.000108	0.000008	0.999998
8	0.000009	0.000001	0.999999
9	0.000006	0	0.999999
10	0.000004	0	1
11	0.000002	0	1
12	0.000001	0	1
13	0.000001	0	1
14	0	0	1

Table S3. Co standard compounds target transformation results of LCLA37 for LCF.

Target materials	Mean squared error
LCO	4.11689E-5
Co_3O_4	3.34936E-4
$CoTiO_3$	2.54132E-4
$LiCoPO_4$	4.1102E-4
Co_2TiO_4	0.00201
CoO	0.00419
$Co(OH)_2$	0.0016
$Co(NO_3)_2\_6H_2O$	0.00927
Co_2P	0.01831
Co metal	0.01437
$CoCO_3$	0.00716
$CoCl_2$	0.00864
CoO(OH)	0.00202
$Co_3(PO_4)_2\_8H_2O$	0.00534

Table S4. Principal component analysis results for Ti K-edge XANES spectra of LCLA37.

Components	Eigenvalues	Variance	Cumulative variance
1	13.95546	0.996819	0.996819
2	0.040105	0.002865	0.999684
3	0.003562	0.000254	0.999939
4	0.000565	0.00004	0.999979
5	0.000168	0.000012	0.999991
6	0.000089	0.000006	0.999997
7	0.000018	0.000001	0.999999
8	0.00001	0.000001	0.999999
9	0.000003	0	1
10	0.000002	0	1
11	0.000002	0	1
12	0.000001	0	1
13	0.000001	0	1
14	0	0	1

Table S5. Ti standard compounds target transformation results of LCLA37 for LCF.

Target materials	Mean squared error
LATP	8.4675E-6
Rutile-TiO_2	1.66967E-4
$CoTiO_3$	7.46717E-4
Co_2TiO_4	0.00252
Amorphous-TiO_2	0.00105
Anatase-TiO_2	0.00116
$Li_4Ti_5O_{12}$	0.00123
Li_2TiO_3	0.00671
Ti_2O_3	0.05307
Ti metal	0.05634

Table S6. Principal-Component Analysis Results for Co K-edge XANES spectra of LCLA55.

Components	Eigenvalues	Variance	Cumulative variance
1	13.85197	0.989426	0.989426
2	0.136191	0.009728	0.999154
3	0.011375	0.000812	0.999967
4	0.00032	0.000023	0.999989
5	0.000065	0.000005	0.999994
6	0.000057	0.000004	0.999998
7	0.00001	0.000001	0.999999
8	0.000005	0	0.999999
9	0.000004	0	1
10	0.000002	0	1
11	0.000001	0	1
12	0.000001	0	1
13	0.000001	0	1
14	0	0	1

Table S7. Co standard compounds target transformation results of LCLA55 for LCF.

Target materials	Mean squared error
LCO	1.08E-05
Co_3O_4	2.43E-04
$CoTiO_3$	0.00131
$LiCoPO_4$	0.00305
Co_2TiO_4	4.74E-4
CoO	0.00453
$Co(OH)_2$	0.01189
$Co(NO_3)_2\_6H_2O$	0.00522
Co_2P	0.01242
Co metal	0.01001
$CoCO_3$	0.01208
$CoCl_2$	0.00576
CoO(OH)	0.00157
$Co_3(PO_4)_2\_8H_2O$	0.00995

Table S8. Principal-Component Analysis Results for Ti K-edge XANES spectra of LCLA55.

Components	Eigenvalues	Variance	Cumulative variance
1	13.92416	0.994583	0.994583
2	0.067259	0.004804	0.999387
3	0.005965	0.000426	0.999814
4	0.00177	0.000126	0.99994
5	0.000554	0.00004	0.99998
6	0.000157	0.000011	0.999991
7	0.000063	0.000005	0.999995
8	0.000038	0.000003	0.999998
9	0.00001	0.000001	0.999999
10	0.000006	0	0.999999
11	0.000005	0	0.999999
12	0.000004	0	1
13	0.000002	0	1
14	0.000001	0	1

Table S9. Ti standard compounds target transformation results of LCLA55 for LCF.

Target materials	Mean squared error
LATP	1.73E-05
Rutile-TiO_2	2.18E-04
$CoTiO_3$	3.00E-04
Amorphous-TiO_2	0.0015
Anatase-TiO_2	0.00368
$Li_4Ti_5O_{12}$	8.21E-04
Co_2TiO_4	4.23E-4
Li_2TiO_3	0.00255
Ti_2O_3	0.04354
Ti metal	0.04925

Table S10. Principal-Component Analysis Results for Co K-edge XANES spectra of LCLA73.

Components	Eigenvalues	Variance	Cumulative variance
1	13.96701	0.997644	0.997644
2	0.032096	0.002293	0.999936
3	0.000597	0.000043	0.999979
4	0.000238	0.000017	0.999996
5	0.000035	0.000003	0.999998
6	0.000017	0.000001	1
7	0.000002	0	1
8	0.000002	0	1
9	0.000001	0	1
10	0.000001	0	1
11	0	0	1
12	0	0	1
13	0	0	1
14	0	0	1

Table S11. Co standard compounds target transformation results of LCLA73 for LCF.

Target materials	Mean squared error
LCO	7.65E-06
Co_3O_4	2.42E-04
$CoTiO_3$	0.0128
$LiCoPO_4$	0.0163
Co_2TiO_4	0.0023
CoO	0.00645
$Co(OH)_2$	0.02761
$Co(NO_3)_2\_6H_2O$	0.01655
Co_2P	0.02454
Co metal	0.02086
$CoCO_3$	0.02864
$CoCl_2$	0.01176
CoO(OH)	0.01015
$Co_3(PO_4)_2\_8H_2O$	0.02636

Table S12. Principal-Component Analysis Results for Ti K-edge XANES spectra of LCLA73.

Components	Eigenvalues	Variance	Cumulative variance
1	13.91641	0.994029	0.994029
2	0.072999	0.005214	0.999243
3	0.007422	0.00053	0.999773
4	0.003042	0.000217	0.999991
5	0.00005	0.000004	0.999994
6	0.000033	0.000002	0.999996
7	0.00002	0.000001	0.999998
8	0.000011	0.000001	0.999999
9	0.000007	0.000001	0.999999
10	0.000004	0	0.999999
11	0.000003	0	1
12	0.000003	0	1
13	0.000001	0	1
14	0.000001	0	1

Table S13. Ti standard compounds target transformation results of LCLA73 for LCF.

Target materials	Mean squared error
LATP	1.33E-05
Rutile-TiO_2	0.00396
$CoTiO_3$	0.00151
Amorphous-TiO_2	0.00139
Anatase-TiO_2	0.00199
$Li_4Ti_5O_{12}$	5.29E-04
Co_2TiO_4	0.00117
Li_2TiO_3	5.55E-04
Ti_2O_3	0.04194
Ti metal	0.04412

2.1. LCF of XANES spectra

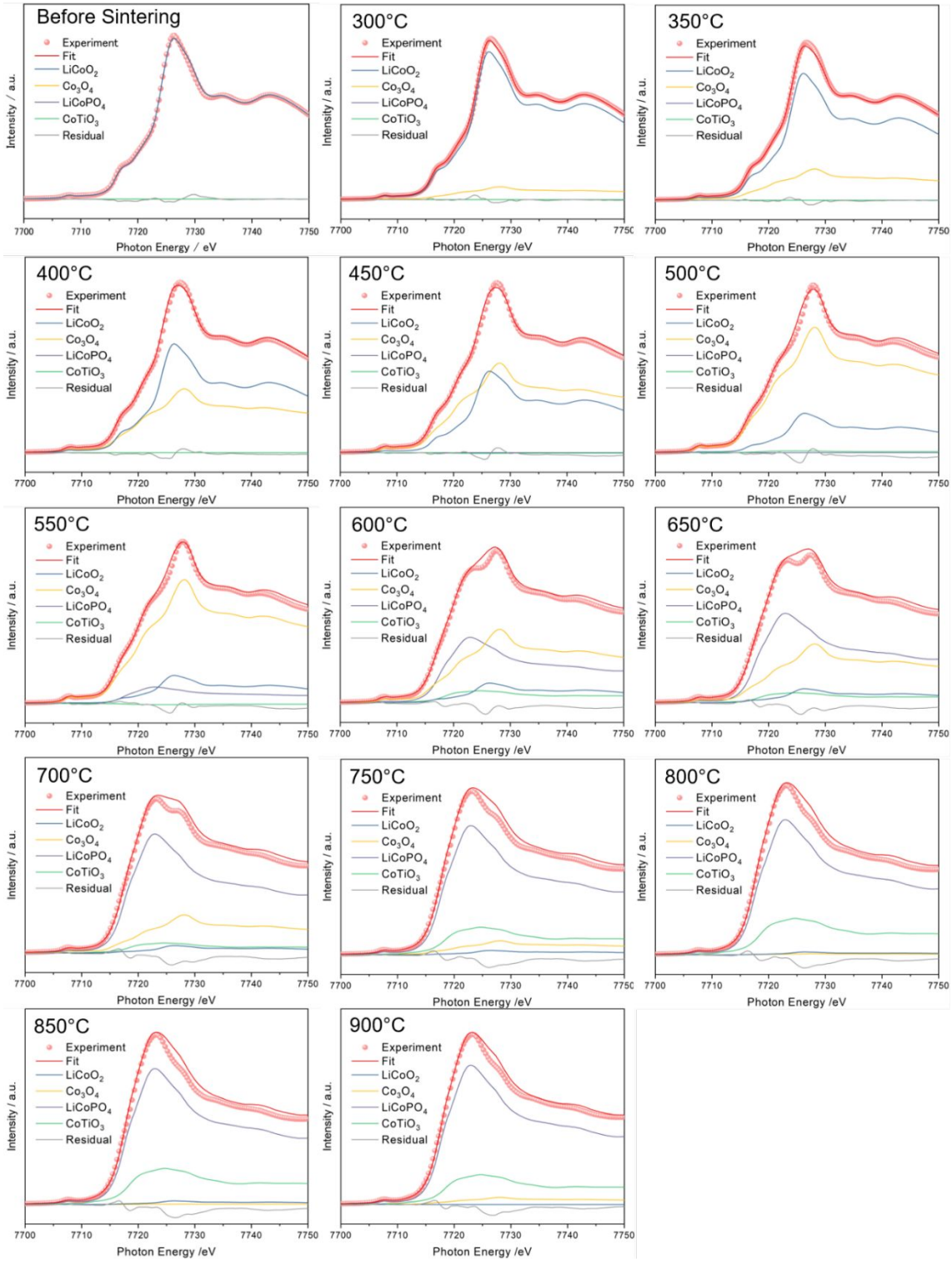

Figure S4. Results of linear combination fitting of the Co K-edge XANES spectra derived from LCLA37.

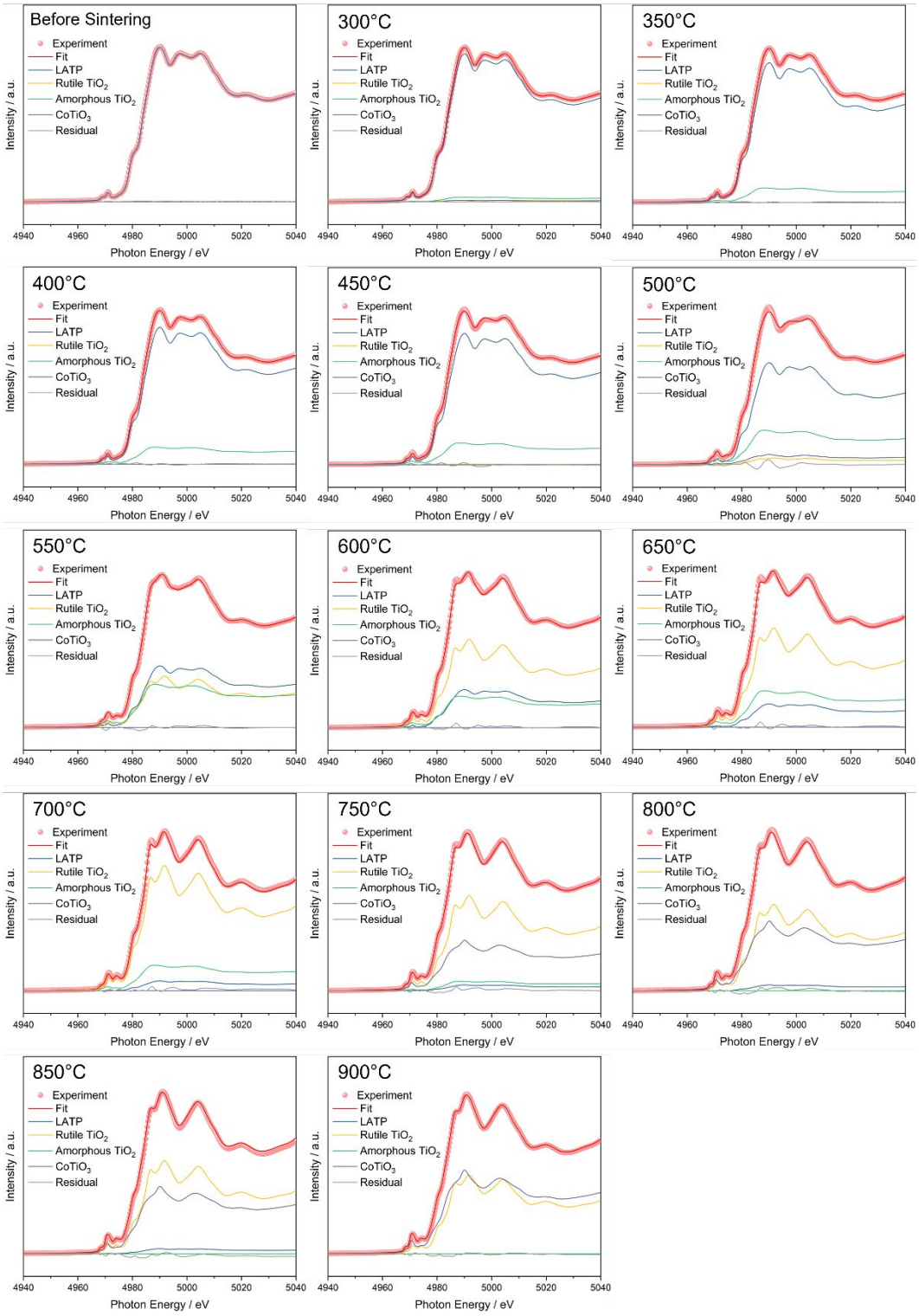

Figure S5. Results of linear combination fitting of the Ti K-edge XANES spectra derived from LCLA37.

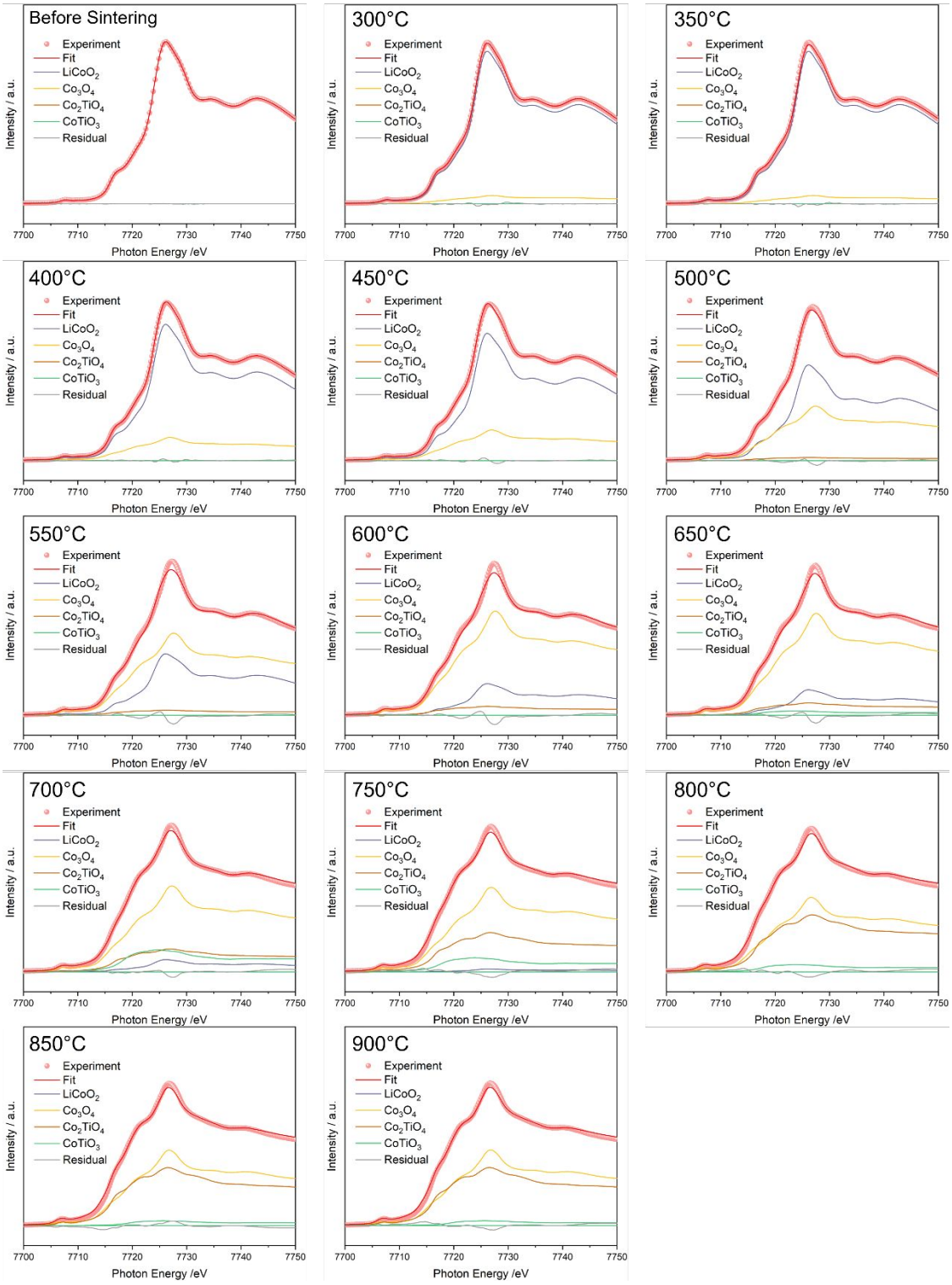

Figure S6. Results of linear combination fitting of the Co K-edge XANES spectra derived from LCLA55.

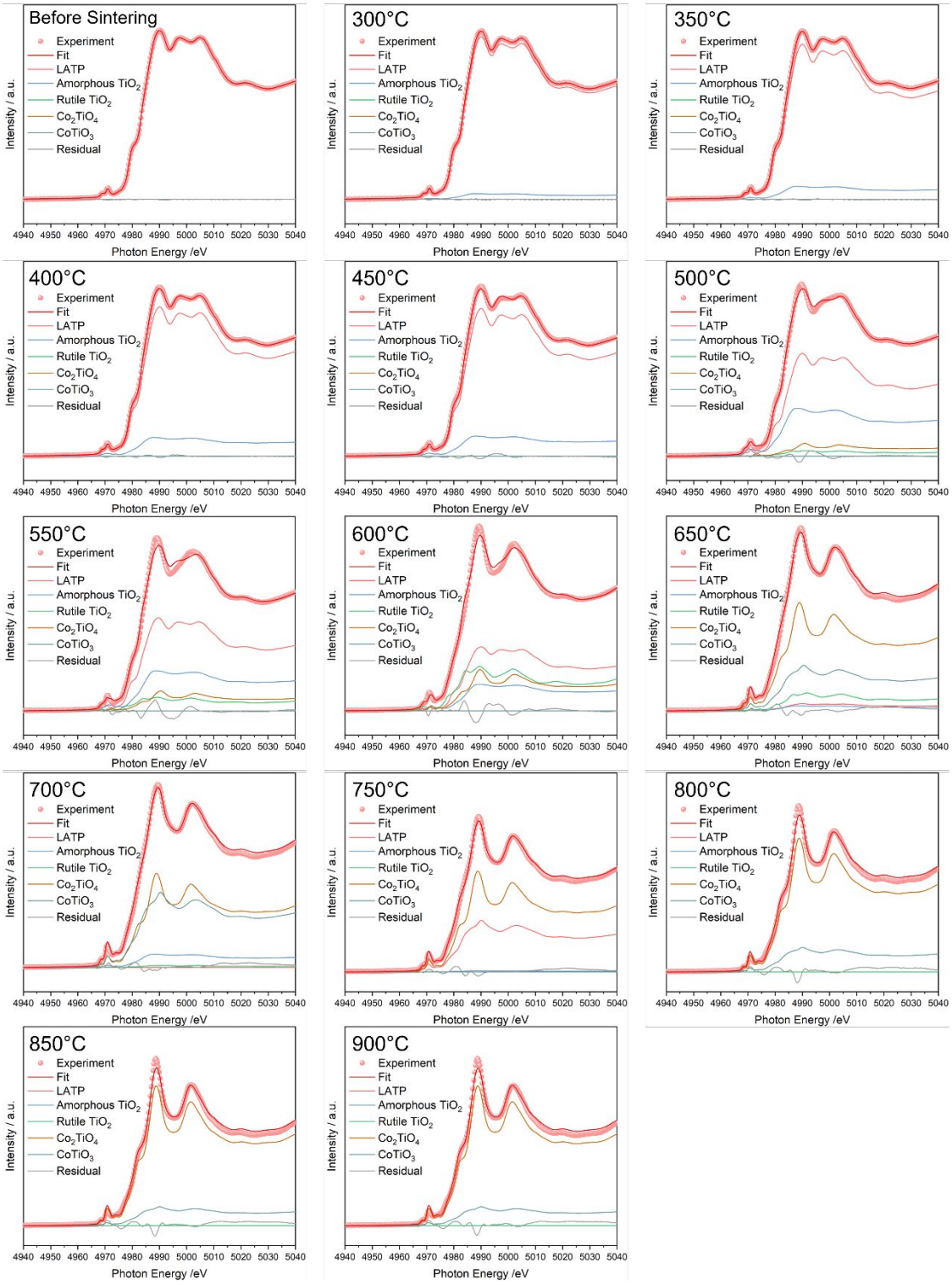

Figure S7. Results of linear combination fitting of the Ti K-edge XANES spectra derived from LCLA55.

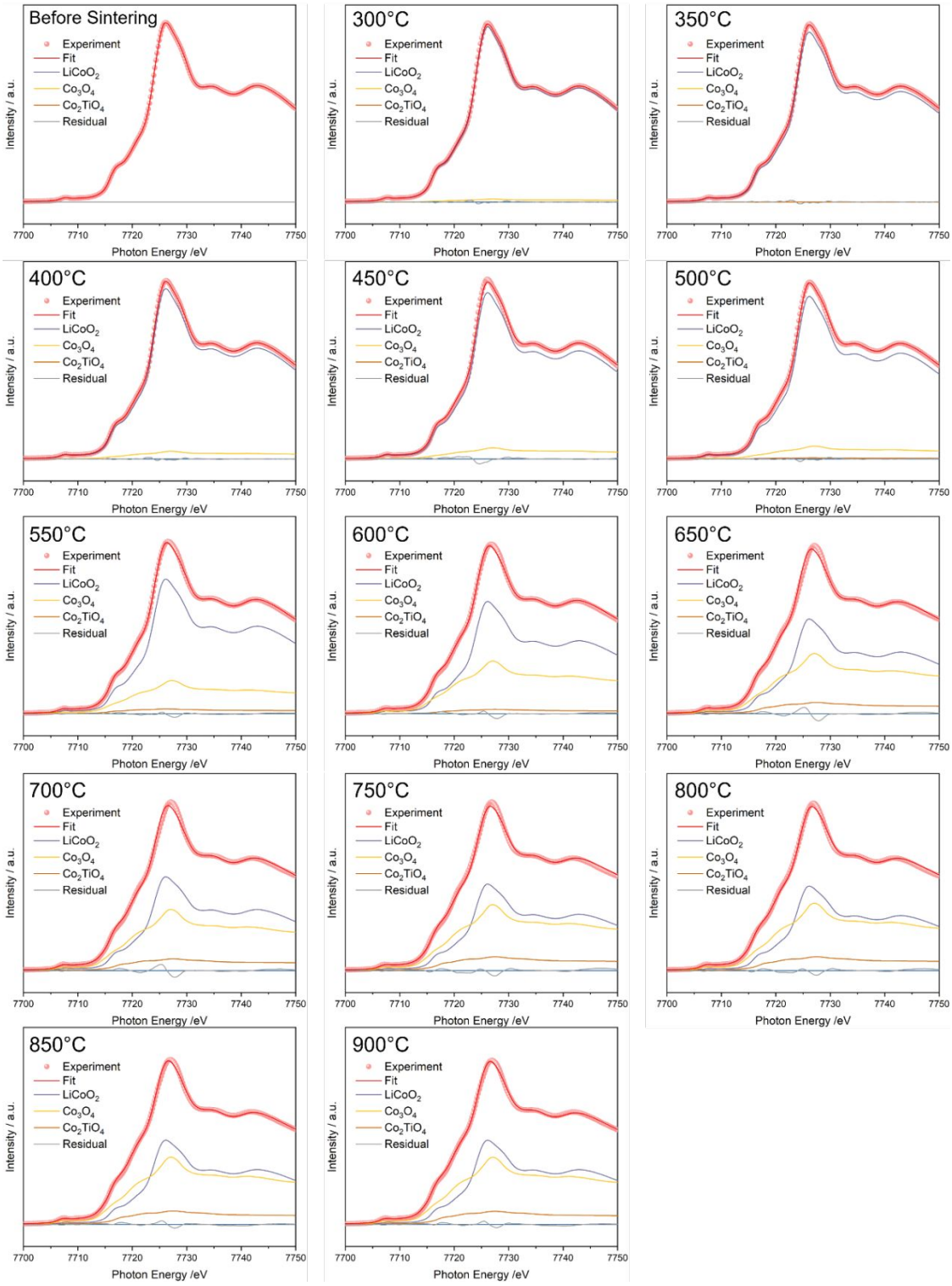

Figure S8. Results of linear combination fitting of the Co K-edge XANES spectra derived from LCLA73.

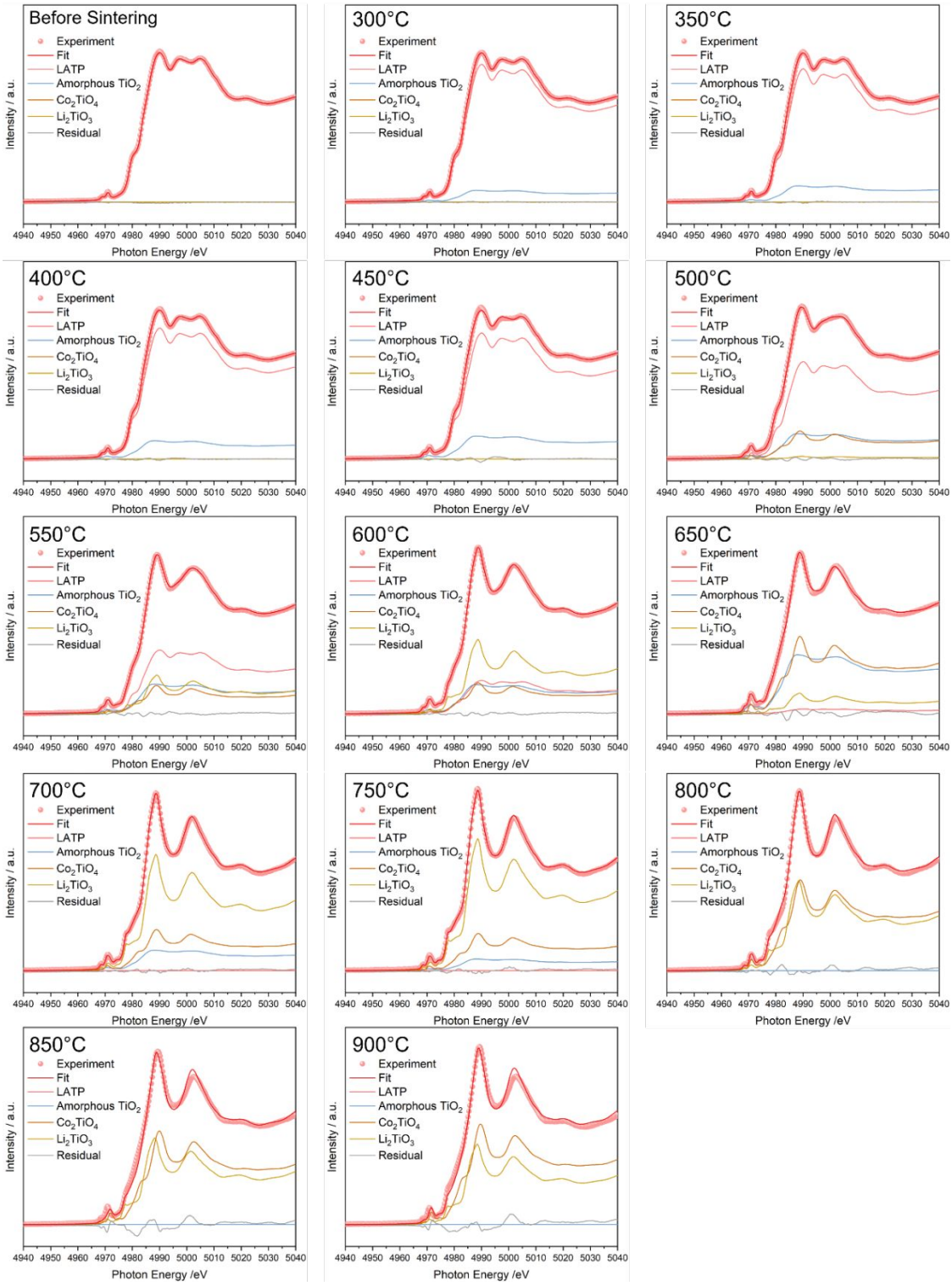

Figure S9. Results of linear combination fitting of the Ti K-edge XANES spectra derived from LCLA73.

3. Ordered and disordered $Li_{4-2x}Co_{3x}Ti_{5-x}O_{12}$ spinel structure and Co_2TiO_4 spinel structure

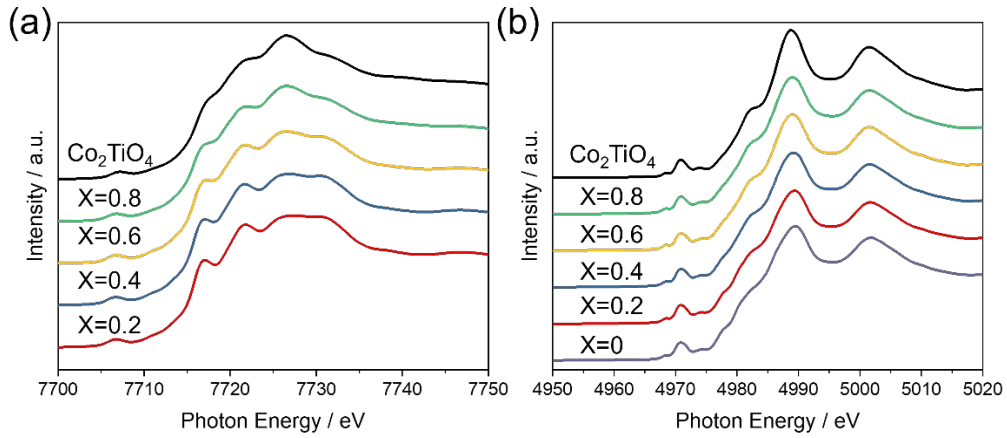

Figure S10. (a) Co K-edge and (b) Ti K-edge XANES spectra of ordered and disordered $Li_{4-2x}Co_{3x}Ti_{5-x}O_{12}$ spinel structure and Co_2TiO_4 spinel structure.

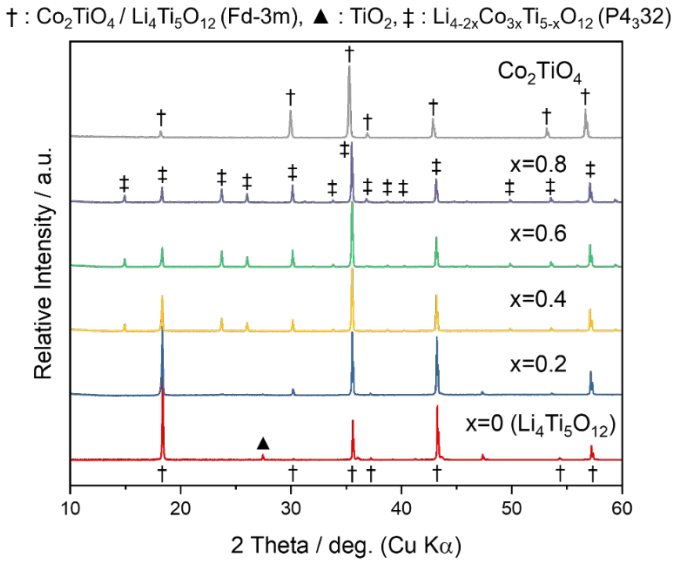

Figure S11. XRD patterns of ordered and disordered $Li_{4-2x}Co_{3x}Ti_{5-x}O_{12}$ spinel structure and Co_2TiO_4 spinel structure.

Co_2TiO_4 was prepared by solid-state reaction method using stoichiometric amount of Co_3O_4 and TiO_2 powder. The mixture of Co_3O_4 and TiO_2 was grinded in a zirconia mortar and pestle and pressed at 2 t/cm^2 in a uniaxial die with a 10 mm diameter to produce a pellet. The pellet was sintered at 1200 °C for 12 h in air.

4. Thermal stability of pure LCO and LATP tested by XRD and XANES

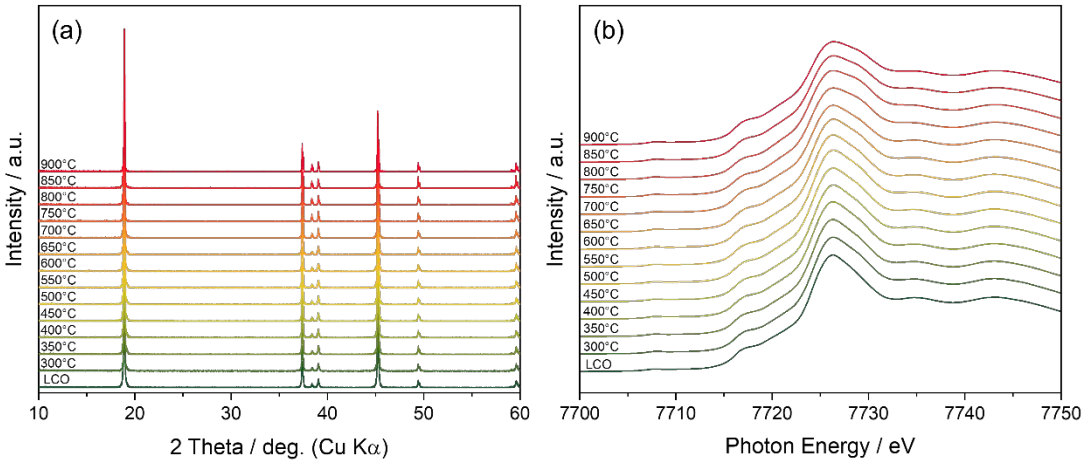

Figure S12. (a) X-ray diffraction patterns and (b) normalized Co K-edge XANES spectra of LCO sintered at various temperatures.

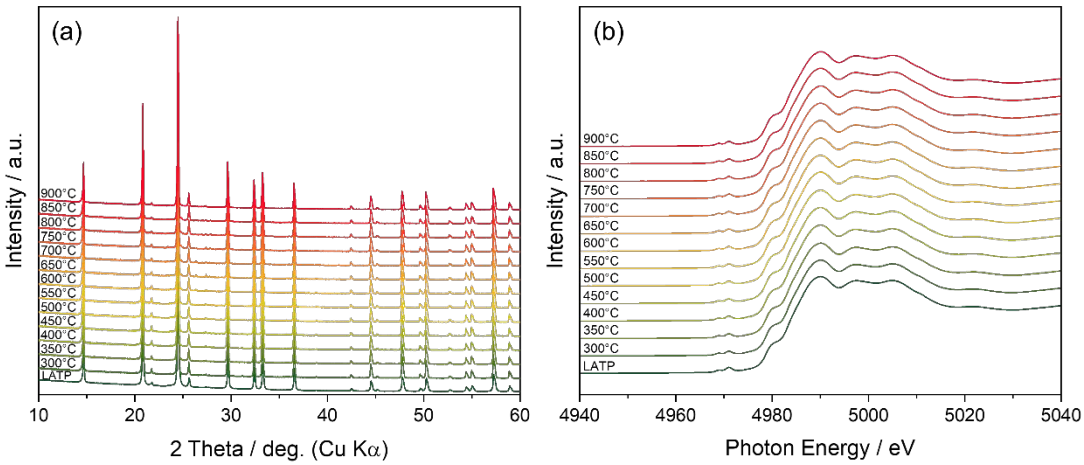

Figure S13. (a) X-ray diffraction patterns and (b) normalized Ti K-edge XANES spectra of LATP sintered at various temperatures.

5. Spinel phase in LCLA55 and LCLA73

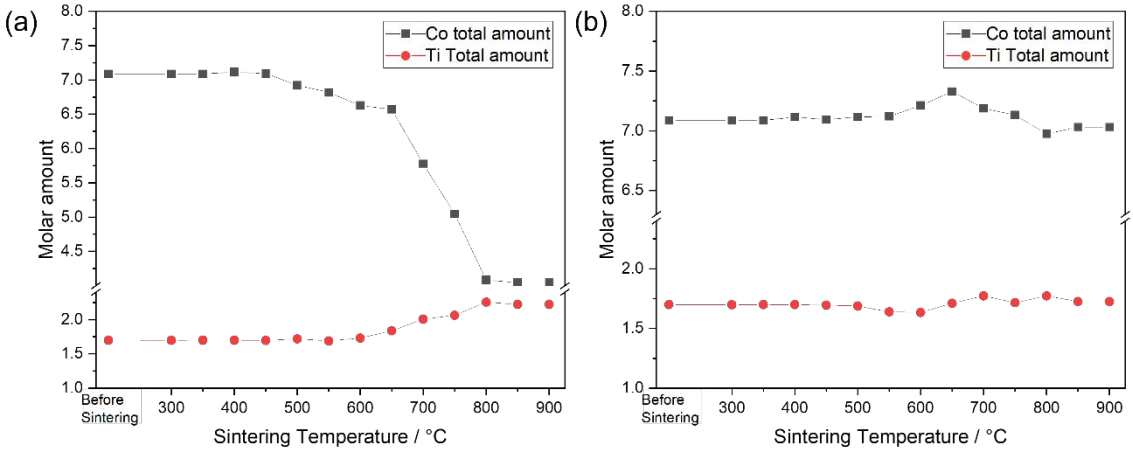

Figure S14. Total amount of Co and Ti cations in LCLA55 calculated for spinel phase as (a) $Li_4Ti_5O_{12}$ and (b) Co_2TiO_4

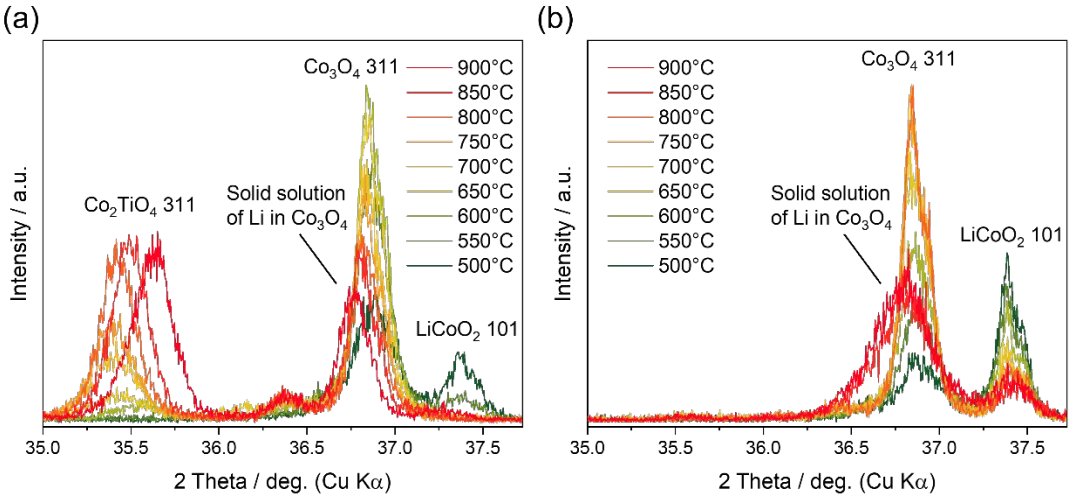

Figure S15. Enlarged the diffraction peaks derived from spinel phases of (a)LCLA55 and (b)LCLA73.

6. Thermodynamics calculation by FactSage 8.2

Table S14. Reaction products observed in experiments and predicted by thermodynamic calculation. (Reaction products written in black color are the reaction products matched by experiment and calculation. Reaction products written in gray color are those calculated as high-temperature phases. Reaction products written in blue color are reaction products considered to be observed as solid solution. Reaction products written in red are those that did not match between experiments.)

	Experimental at 900 °C	**Calculation at 900 °C**
LCLA37	$LiCoPO_4$, $CoTiO_3$, TiO_2, Li_3PO_4	$LiCoPO_4$, TiO_2, Li_3PO_4, $CoTi_2O_5$
LCLA55	Co_3O_4, $CoTiO_3$,Co_2TiO_4, Li_3PO_4	$LiCoPO_4$, CoO, $Li_2CoTi_3O_8$, Li_3PO_4
LCLA73	$LiCoO_2$, Co_3O_4, Li_3PO_4, Co_2TiO_4, Li_2TiO_3	$LiCoO_2$, CoO, $Li_2CoTi_3O_8$, Li_3PO_4, Li_2TiO_3
	Experimental at 800 °C	**Calculation at 800 °C**
LCLA37	$LiCoPO_4$, $CoTiO_3$, TiO_2, Li_3PO_4	$LiCoPO_4$, TiO_2, Li_3PO_4, $CoTi_2O_5$
LCLA55	Co_3O_4, $CoTiO_3$, Co_2TiO_4, Li_3PO_4	$LiCoPO_4$, CoO, $CoTi_2O_5$, Li_3PO_4
LCLA73	LCO, Co_3O_4, Li_3PO_4, Co_2TiO_4, Li_2TiO_3	LCO, CoO, $Li_2CoTi_3O_8$, Li_3PO_4
	Experimental at 700 °C	**Calculation at 700 °C**
LCLA37	LATP, $LiCoPO_4$, $CoTiO_3$, TiO_2, Li_3PO_4	$LiCoPO_4$, TiO_2, Li_3PO_4, $CoTi_2O_5$
LCLA55	Co_3O_4, $CoTiO_3$, Co_2TiO_4, TiO_2, Li_3PO_4	$LiCoPO_4$, CoO, $CoTi_2O_5$, Li_3PO_4
LCLA73	LCO, Co_3O_4, Li_3PO_4, Li_2TiO_3	LCO, CoO, $Li_2CoTi_3O_8$, Li_3PO_4
	Experimental at 600 °C	**Calculation at 600 °C**
LCLA37	LCO, LATP, Co_3O_4, amo-TiO_2, TiO_2, $LiCoPO_4$, Li_3PO_4	$LiCoPO_4$, TiO_2, Li_3PO_4, $CoTi_2O_5$
LCLA55	LATP, Co_3O_4, $CoTiO_3$, Co_2TiO_4, amo-TiO_2 TiO_2, Li_3PO_4	$LiCoPO_4$, Co_3O_4, $CoTi_2O_5$, Li_3PO_4
LCLA73	LCO, LATP, Co_3O_4, Li_3PO_4, Li_2TiO_3, amo-TiO_2	$Li_{0.5}CoO_2$, Co_3O_4, $Li_2CoTi_3O_8$, Li_3PO_4
	Experimental at 500 °C	**Calculation at 500 °C**
LCLA37	LCO, LATP, Co_3O_4, amo-TiO_2 ,TiO_2, $LiCoPO_4$, Li_3PO_4	$LiCoPO_4$, TiO_2, Li_3PO_4, $CoTi_2O_5$
LCLA55	LATP, Co_3O_4, $CoTiO_3$, Co_2TiO_4, amo-TiO_2 TiO_2, Li_3PO_4	$LiCoPO_4$, Co_3O_4, $CoTi_2O_5$, Li_3PO_4
LCLA73	LCO, LATP, Co_3O_4, Li_3PO_4, Li_2TiO_3, amo-TiO_2	$Li_{0.5}CoO_2$, LCO, $Li_2CoTi_3O_8$, Li_3PO_4

7. LCLA37 sintering experiments with varying sintering time and particle size.

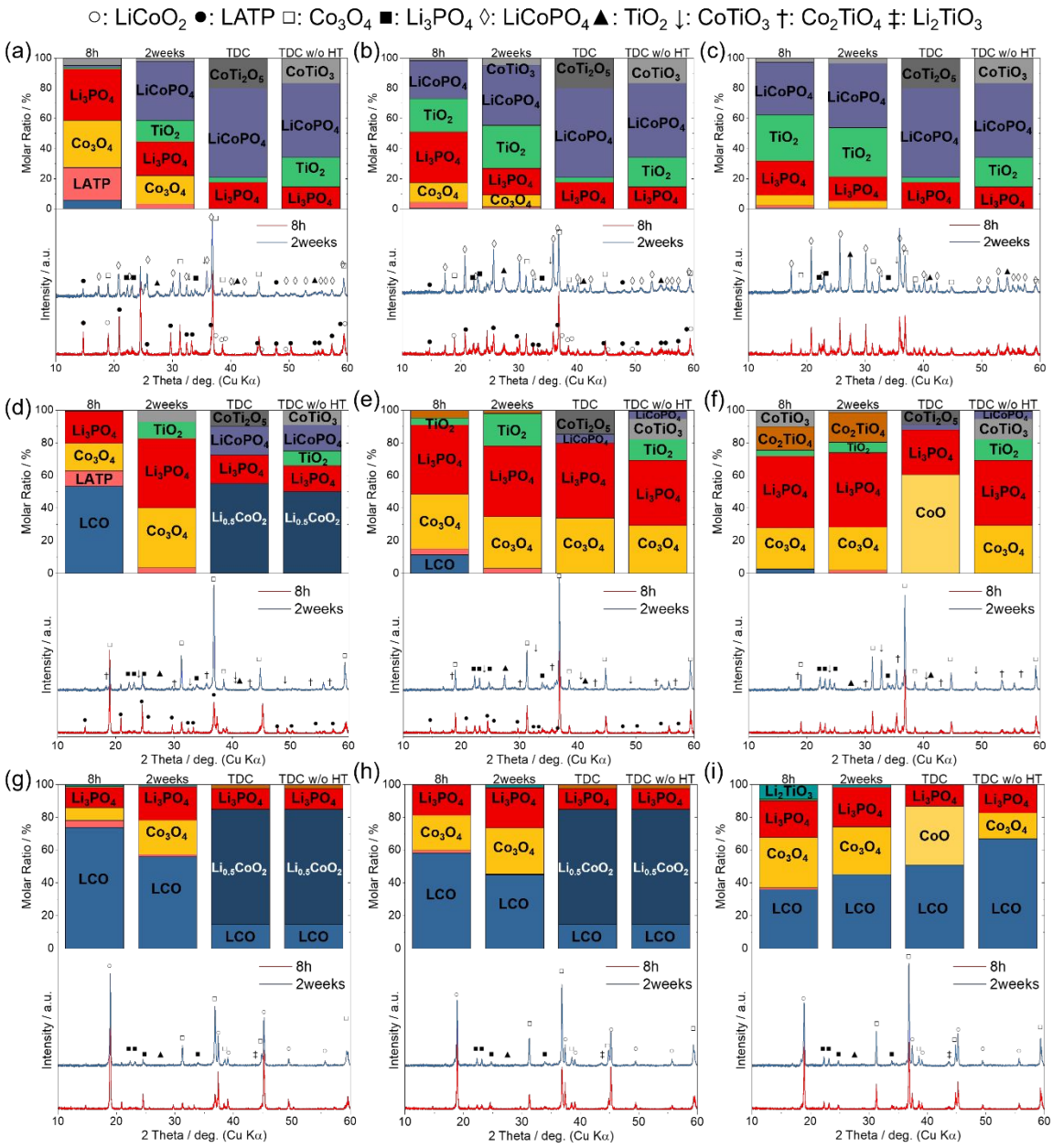

Figure S16. XRD patterns and Rietveld analysis results of LCLA37 sintered at (a) 500°C, (b) 600°C and (c) 700°C for 8 hours and 2 weeks. XRD patterns and Rietveld analysis results of LCLA55 sintered at (d) 500°C, (e) 600°C and (f) 700°C for 8 hours and 2 weeks. XRD patterns and Rietveld analysis results of LCLA73 sintered at (g) 500°C, (h) 600°C and (i) 700°C for 8 hours and 2 weeks. The Rietveld analysis results are shown together with the thermodynamic calculation (TDC) results and the thermodynamic calculation results without the high temperature phase (TDC w/o HT).

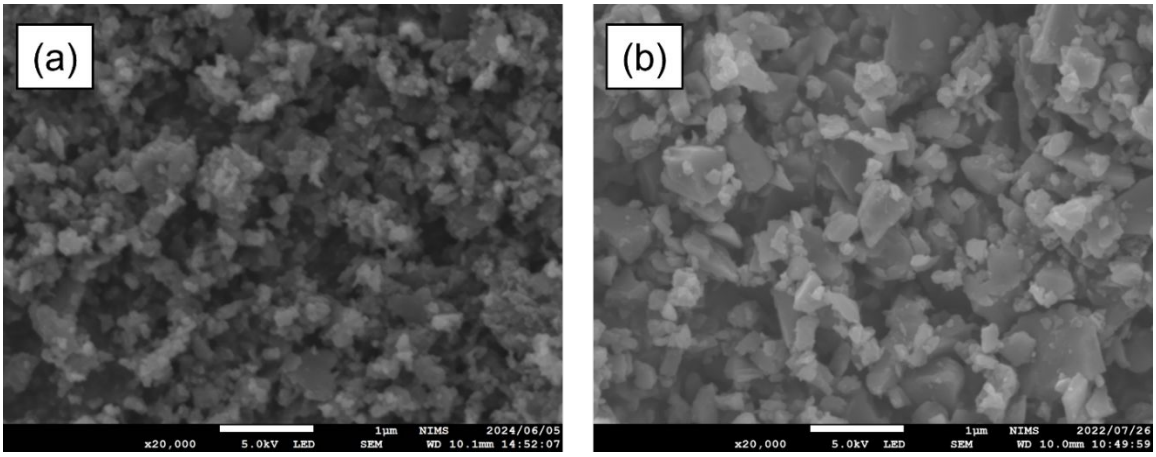

Figure S17. (a) SEM image of (a) fine and (b) regular grain LATP.

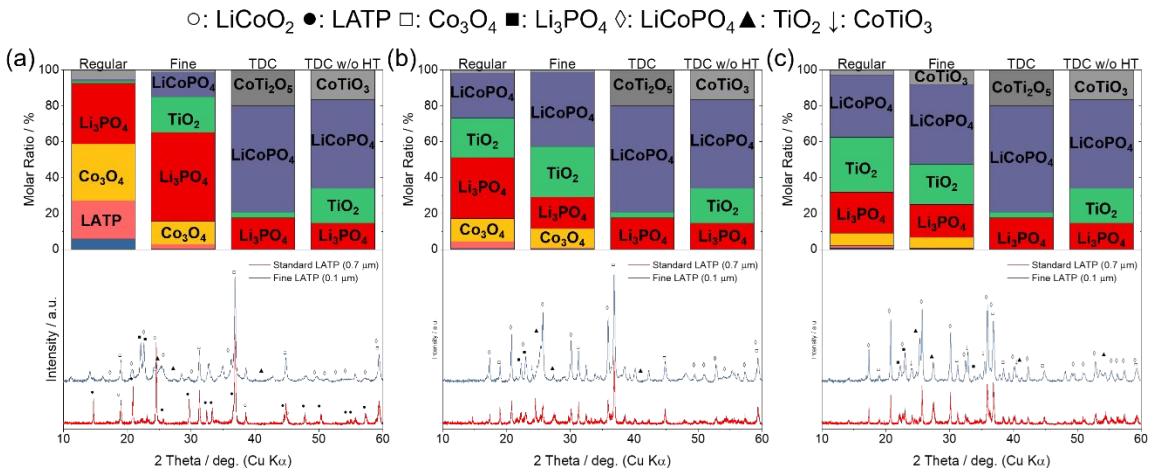

Figure S18. XRD patterns and Rietveld analysis results of LCLA37 sintered at (a) 500°C, (b) 600°C and (c) 700°C using fine and regular grain LATP. The Rietveld analysis results are shown together with the thermodynamic calculation (TDC) results and the thermodynamic calculation results without the high temperature phase (TDC w/o HT).

8. Molar amount of thermodynamically stable phase of LCLA55

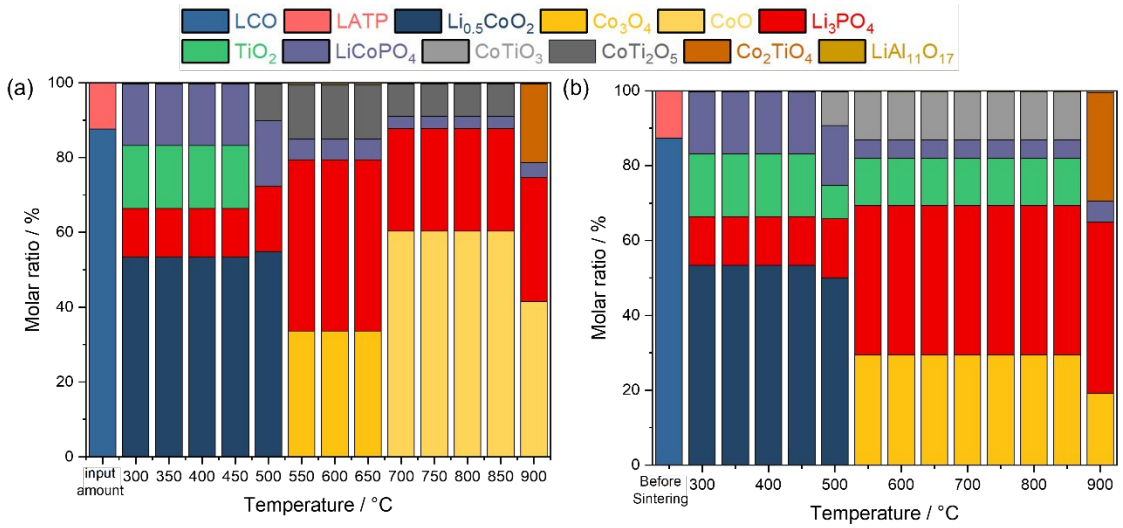

Figure S19. (a) Molar amount of thermodynamically stable phase of LCLA55 after replacing $LiCoPO_4$, $Li_2CoTi_3O_8$ and 4CoO with Li_3PO_4 and $3Co_2TiO_4$ and (b) subsequent conversion of the high temperature phase to the low temperature phase.